Investigation of Mixed Convection in a Vertical Microchannel Affected by EDL

H. Shokouhmand, A. Jafari

Abstract— A problem of mixed convection in a vertical micro channel affected by an applied electrical potential with symmetric wall temperature is studied numerically. A non linear two-dimensional Poisson equation governing the applied electrical potential and zeta potential of solid-liquid boundary and Nersent-Plank equation governing the ionic concentration distribution are numerically solved using a finite volume method. Body forces caused by the interaction between the charge density and applied electrical potential field and buoyancy effect are included in the full Navier-Stokes equation. The SIMPLE algorithm is employed to solve the corresponding numerical equations formulated by the finite-volume method. The governing equations are discretized using a control volume approach on a staggered mesh and a pressure correction method is employed for the pressure–velocity coupling. A hybrid scheme is used to model the convective term, and a suitable grid distribution is introduced. Because of high velocity gradient in microchannels viscous dissipation is also considered. It is found that by increasing the Re number while keeping the electrical potential constant, the flow tends to poiselluie flow and consequently the local Nusselt number decreases. It is also observed that increasing the Grashof number has insignificant effect on fluid flow and heat transfer.

Keywords— Finite volume, Poisson equation, SIMPLE method, Vertical microchannel, Viscous dissipation.

I. INTRODUCTION

Recent developments in microfabrication technologies have enabled a variety of miniaturized fluidic systems, which can be utilized for medical, pharmaceutical, defense, and environmental monitoring applications. Examples of such applications are drug delivery, DNA analysis/sequencing systems and biological/chemical agent detection sensors on microchips. Along with the necessary sensors and electronic units, these devices include various fluid handling components such as microchannels, pumps, and valves. Utilization of electrokinetic body forces in microfluidic design can revolutionize various fluid handling applications, since it will be possible to build flow control elements with *nonmoving components* [1].

Among these applications, *electro-osmosis* based *MEMS* are one of the most favored setups due to its ease of fabrication, accuracy of flow control and absence of moving parts [2]-[3]. Electro-osmosis is a basic electrokinetic phenomenon, where the flow of an electrolyte in a channel is induced by an external electric field applied between the inlet and outlet, after the interaction between the dielectric channel walls and the polar fluid has created near-wall layers of counter-ions within the fluid [4]. These layers of liquid move under the action of the applied electric field whereas the neutral core is dragged and moves as a solid body [5].The principle was first demonstrated by Reuss in 1809 [6] in an experimental investigation using porous clay. This was followed by the theoretical work on the electric double layer (EDL) of Helmholtz in 1879 [7], which related the electrical and flow parameters for electro-kinetically driven flows. In the early 1900s von Smoluchowski [8] contributed to the under-standing of electrokinetically driven flows, especially for conditions where the EDL thickness is much smaller than the channel height. Mala et al. [9] studied the effects of EDL on fluid flow and heat transfer through a parallel-plate microchannel, and Li et al. [10]-[11] studied the electro-osmotic flows in rectangular microchannels. In the both works, analytical solutions were obtained with the help of the classical Debye–Huckel approximation. Hu et al [12] developed a numerical scheme to study the electroosmotic flow in intersecting channels in a T-shaped configuration. Yang et al [13]-[14]. And Arulanandam and Li [15] used numerical methods to simulate fluid flow through a microchannel. Their physical models were based on the Poisson–Boltzmann equation for the EDL potential, the Laplace equation for the applied electrostatic field, and the Navier–Stokes equations modified to include effects of the body force by the interaction between electrical and zeta potential. Their numerical results of the model are in qualitative agreement with their experimental observations [16].

Mixed convection: Geng and Chen [17] studied the problem of mixed convection in a vertical channel with asymmetric wall temperatures including situations of flow reversal. A comparison between their numerical solutions and those in Aung and Worku [18] indicates that the marching technique using the boundary-layer equations accurately calculate the heat transfer on the heated wall. Avci and Aydin [19] presented an analytical solution for fully developed mixed convective heat transfer of a Newtonian fluid in an open-

Manuscript received November 2, 2009. The 2010 International Conference of Mechanical Engineering (ICME'10)
H.Shokouhmand, Professor of School *of Mechanical Engineering, College of Engineering, University of Tehran, Tehran, Iran* (e-mail: hshokoh@ ut.ac.ir).
A.Jafari, M.S. student School *of Mechanical Engineering, College of Engineering, University of Tehran, Tehran, Iran* (corresponding author to provide phone: 00989355687704; e-mail: arianjafari@ ut.ac.ir).

ended vertical parallel plate microchannel with asymmetric wall heating at uniform heat fluxes. They found that increasing Gr_q/Re from 1 to 200 will lead to an increase of ≈2% in *Nu*. A. Barletta and Celli [20] investigated combined forced and free flow in a vertical channel with an adiabatic wall and an isothermal wall.

Previous studies of electroosmotic flow have presented results for velocity distribution and the friction coefficient. They are limited to fully developed flow in microchannels under very low Reynolds number. In this paper, our physical model is different from that in the previous studies, namely, (1) the computational domain is considered from entry region to fully developed region, and (2) also the full Navier–Stokes equations including convection term, pressure gradient term, and body force term is considered. The force in the case of electroosmotic flow includes not only body force but also pressure gradient term to balance the shear stress in the fluid and buoyancy force. Therefore, full terms in the momentum equations are involved.

II. GOVERNING EQUATIONS

Fig. 1 shows the examined model of the liquid flow in a vertical microchannel between two parallel plates, which are separated by a distance L. Constant temperatures, T_h at the right and left walls are imposed. The fluid is assumed to be incompressible, with constant physical properties. The buoyancy effects on momentum transfer are taken into account through the Boussinesq approximation. Viscous dissipation is also considered.

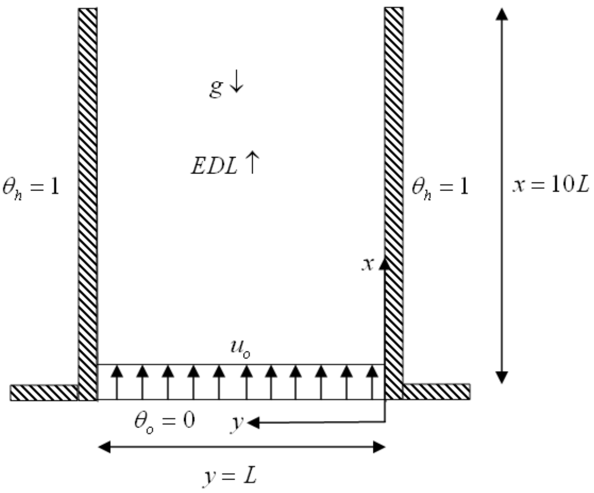

Fig. 1, Physical model affected by EDL

The zeta potential at the right and left walls are depicted horizontally for ease in Figs. (2-6). According to the theory of electrostatics, the relationship between the electrical potential ψ and the local net charge density per unit volume ρ_e at any point in the solution is described by the Poisson equation:

$$\nabla^2\psi = -\frac{\rho_e}{\varepsilon\varepsilon_o} \tag{1}$$

Where ε is the dielectric constant of the medium and ε_o is permittivity of vacuum. Assuming the equilibrium, Boltzmann distribution equation is applicable which implies uniform dielectric constant; the number concentration of the type-i ion in a symmetric electrolyte solution is of the form:

$$n_i = n_{io}\exp\left(\frac{z_i e\psi}{k_B T}\right) \tag{2}$$

where n_{io} and z_i are the bulk concentration and the valence of type-i ions, respectively, e is the charge of a proton, k_b is the Boltzmann constant, and T is the absolute temperature. The net volume charge density ρ_e is proportional to the concentration difference between symmetric cations and anions, with:

$$\rho_e = ze(n_+ - n_-) = -2zen_o\sinh\left(\frac{ze\psi}{k_b T}\right) \tag{3}$$

Substituting Eq. (3) into the Poisson equation, Eq. (1) leads to the well-known Poisson–Boltzmann equation.

$$\frac{\partial^2\psi}{\partial^2 x} + \frac{\partial^2\psi}{\partial^2 y} = \frac{2zen_o}{\varepsilon\varepsilon_o}\sinh\left(\frac{ze\psi}{k_b T}\right) \tag{4}$$

By defining the Debye–Huckel parameter $k^2 = 2z^2e^2n_o/k_bT$ ($1/k$ is normally referred to as the EDL thickness) and introducing the dimensionless groups:x/L,y/L,$ze\psi/k_bT$, Eq.(4) can be non-dimensionlized as:

$$\frac{\partial^2\Psi}{\partial^2 x^*} + \frac{\partial^2\Psi}{\partial^2 y^*} = k^2\sinh(\Psi) \tag{5}$$

For large values of ψ , the linear approximation is no longer valid. The EDL field has to be determined by solving Eq. (10). In order to solve this non-linear, two-dimensional, differential equation, a numerical finite-volume scheme may be introduced to derive this differential equation into the discrete, algebraic equations by integrating the governing differential equation over a control volume surrounding a typical grid point. The non-linear source term is linearized as:

$$\sinh\Psi_{n+1} = \sinh\Psi_n + (\Psi_{n+1} - \Psi_n)\cosh\Psi_n \tag{6}$$

where the subscript (n+1) and n represent the (n+1) th and the nth iterative value, respectively.

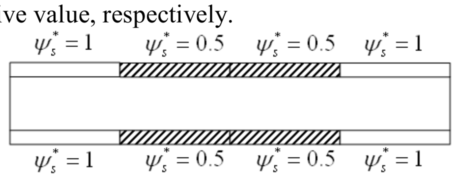

Fig. 2, Zeta potential arrangement case 1

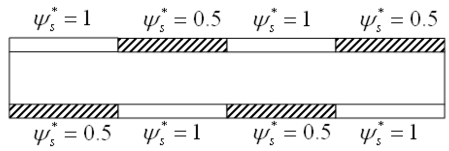

Fig. 3, Zeta potential arrangement case 2

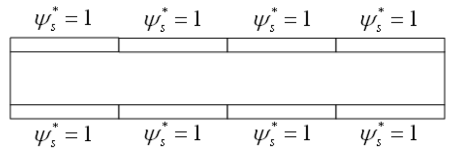

Fig. 4, Zeta potential arrangement case 3

ISBN: 978-988-18210-7-2
ISSN: 2078-0958 (Print); ISSN: 2078-0966 (Online)

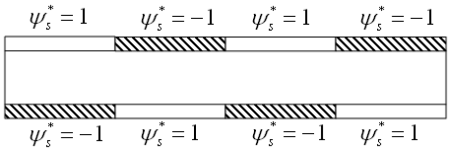

Fig. 5, Zeta potential arrangement case 4

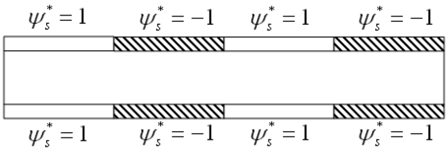

Fig. 6, Zeta potential arrangement case 5

Finally by introducing following non-dimensional terms:

$$x^* = \frac{x}{L} \quad , y^* = \frac{y}{L}, \quad u^* = \frac{u}{u_o}, \quad v^* = \frac{v}{u_o}$$

$$p^* = \frac{p}{\rho u_o^2}, \quad , \quad \theta = \frac{T - T_o}{T_h - T_o} \tag{7}$$

$$Gr = \frac{g\beta L^3 (T_h - T_o)}{\upsilon^2}, \ \mathrm{Re} = \frac{u_o L}{\upsilon} \ , Pe = \mathrm{Re.Pr}$$

$$Ec = \frac{u_o^2}{c_p (T_h - T_o)}, E_x = \frac{EL}{\zeta}, G = \frac{2zen_o \zeta}{\rho u_o^2}$$

The non-dimensional continuity, momentum, and energy equations will be obtained (for simplicity we have omitted stars) as:

Continuity equation:

$$\frac{\partial u}{\partial x} + \frac{\partial v}{\partial y} = 0 \tag{8}$$

U-momentum equation:

$$u\frac{\partial u}{\partial x} + v\frac{\partial u}{\partial y} = -\frac{\partial p}{\partial x} + \frac{1}{\mathrm{Re}}\left(\frac{\partial^2 u}{\partial^2 x} + \frac{\partial^2 u}{\partial^2 y}\right) + \\ + \frac{Gr}{\mathrm{Re}^2}\theta + G\overline{E}_x \sinh\left(\psi^*\right) \tag{9}$$

V-momentum equation:

$$u\frac{\partial v}{\partial x} + v\frac{\partial v}{\partial y} = -\frac{\partial p}{\partial y} + \frac{1}{\mathrm{Re}}\left(\frac{\partial^2 v}{\partial^2 x} + \frac{\partial^2 v}{\partial^2 y}\right) \tag{10}$$

Energy equation:

$$u\frac{\partial \theta}{\partial x} + v\frac{\partial \theta}{\partial y} = \frac{1}{Pe}\left(\frac{\partial^2 \theta}{\partial^2 x} + \frac{\partial^2 \theta}{\partial^2 y}\right) + \\ + \frac{Ec}{\mathrm{Re}}\left(2\left[\left(\frac{\partial u}{\partial x}\right)^2 + \left(\frac{\partial v}{\partial y}\right)^2\right] + \left(\frac{\partial u}{\partial y} + \frac{\partial v}{\partial x}\right)^2\right) \tag{11}$$

The boundary conditions are as follows:

1. At the surface of each plate (walls):

$$u = v = 0 \quad , \quad \theta = 1 \tag{12}$$

2. At the entrance:

$$u = 1 \quad , v = 0 \quad , \quad \theta = 0 \tag{13}$$

3. At the exit:

$$\frac{\partial u}{\partial x} = 0 \ , v = 0 \quad , \quad \frac{\partial \theta}{\partial x} = 0 \tag{14}$$

These mean that at the exit, fully developed conditions are considered.

III. NUMERICAL METHOD

The governing equations are solved by finite-volume method. The SIMPLE full-staggered algorithm for the solution of the Navier–Stokes and energy equations can be summarized by the following steps:

1. Guess p
2. Solving momentum equations and finding u, v
3. Solving pressure correction equation and obtaining the modified u, v, p .
4. Calculation of residual term in pressure correction equation (if it is equal to zero, the solution has been converged).
5. Calculation of energy equation or any other scalar equation.
6. Repeating steps (2-5) till the convergence criteria is satisfied.

By applying the SIMPLE algorithm, the governing equations become as follows:

Step 2:

$$A_p u_p = \sum_{nb} A_{nb} u_{nb} + \left(p_{I-1,J} - p_{I,J}\right)\left(y_\eta\right)_{cell} \Delta\eta\Delta\xi + \\ + Sc \times \Delta\eta\Delta\xi \tag{15}$$

$$Sc = \left(J \times source\right)_{cell}$$

Step 4:

$$b_{I,J} = \left(u_{i+1,J} - u_{i,J}\right)\left(y_\eta\right)_{cell}\Delta\eta - \left(v_{I,j+1} - v_{I,j}\right)\Delta\xi \tag{16}$$

Step 5:

$$A_p \theta_p = \sum_{nb} A_{nb}\theta_{nb} + \frac{Ec}{\mathrm{Re}^2} J \times \Delta\eta\Delta\xi \tag{17}$$

In above equation J indicates *Jacobian* for transform matrix. Because of high velocity gradient at walls, we use a non-uniform grid to reduce the time of calculations. This grid is depicted in Fig. (7). The below transformation function is used to cluster the mesh near the two walls:

$$y = L\frac{(2\alpha + \beta)\left[\frac{(\beta+1)}{(\beta-1)}\right]^{\frac{\eta-\alpha}{1-\alpha}} + 2\alpha - \beta}{(2\alpha+1)\left\{1 + \left[\frac{(\beta+1)}{(\beta-1)}\right]^{\frac{\eta-\alpha}{1-\alpha}}\right\}} \tag{18}$$

ISBN: 978-988-18210-7-2
ISSN: 2078-0958 (Print); ISSN: 2078-0966 (Online)

Where β is the clustering parameter, and α defines where the clustering takes place. When $\alpha = 0$, the clustering is a $y = L$ whereas, when $\alpha = 1/2$, clustering is distributed equally at $y = 0$ and $y = L$. In this paper, β is set at 1.03.

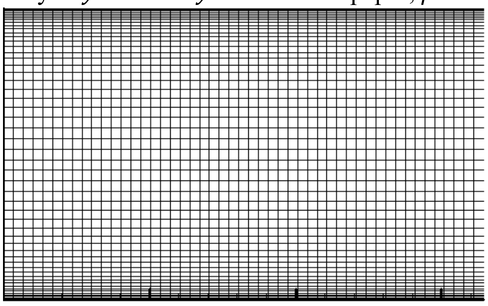

Fig. 7, Physical domain mesh

IV. RESULT AND DISCUSSION

The fluid is considered water with Pr = 5.66. The effects of parameters of Reynolds number, Grashof number and five type of zeta potential arrangement are examined.

The numerical solution is validated by applying the method on mixed convection through a vertical macro channel. A comparison is performed between the obtained results and those presented experimentally by Aung et al. As observed in Fig. , they are in good agreement.

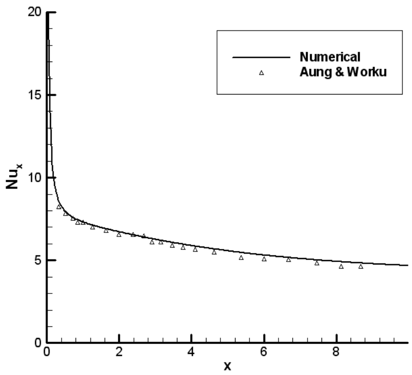

Fig. 8, Comparison between numerical and experimental Nu

For four case studied, the velocity profile are demonstrated in Figs. (9-12). As shown by increasing Reynolds number in a constant zeta potential distribution, G, and E, the power of EDL near the walls reduces and velocity profile tends to be like a poiseuille flow. In the fourth and fifth case, the minus zeta potential makes flow reversal; this effect can be useful when the fluid mixture is desired.

Consider the microchannels with a width L=30(μm), a length x=10L. The external electrical field strength along the x direction is E_x =100(V/cm), the ionic concentration n_∞ =10^{-6} (M), and the other parameters include: the dynamic viscosity μ= 0.9×10^{-3} (Nsm^{-2}), density ρ =1.0×103(kgm^{-3}), the dielectric constant of the solution ε = 80, the permittivity of vacuum ε_o = 8.854×10^{-12}($C^2\ J^{-1}m^{-1}$), the Boltzmann constant k_B= 1.38×10^{-23} ($J\ K^{-1}$), the charge of a proton e =1.6×10^{-19}(C), the temperature T = 298(K), zeta potential on the channel wall ζ=−25(mV).

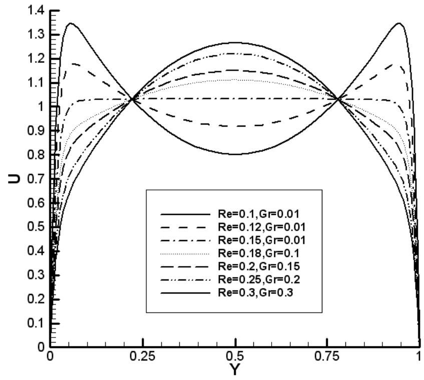

Fig. 9, Fully-developed velocity profile in case 1, 3

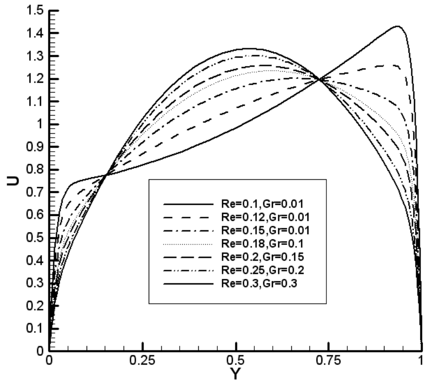

Fig. 10, Fully-developed velocity profile in case 2

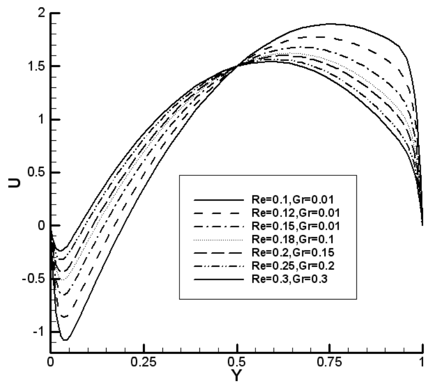

Fig. 11, Fully-developed velocity profile in case 4

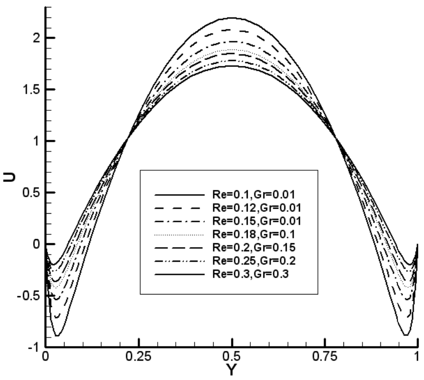

Fig. 12, Fully-developed velocity profile in case 5

The local Nusselt number is calculated by the following equation:

$$Nu_x = \frac{1}{1-\theta_b} \frac{\partial \theta}{\partial y}\bigg|_{y=0} \tag{19}$$

In this study we use a structured-clustered mesh with 55×300 nodes for all cases. Figs. (13-17) show the variations of local Nusselt number through the microchannel for five studied zeta potential arrangements.

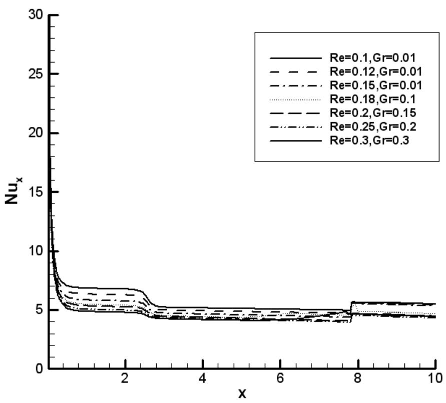

Fig. 13, Local Nusselt number through microchannl in case 1

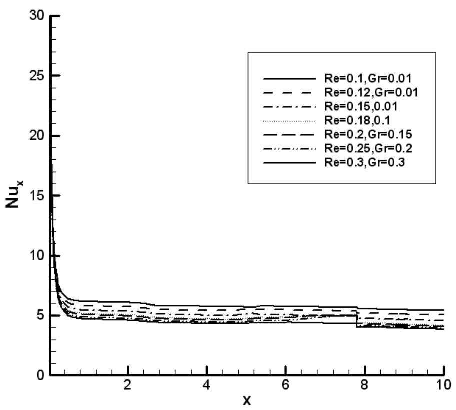

Fig. 14, Local Nusselt number through microchannel in case 2

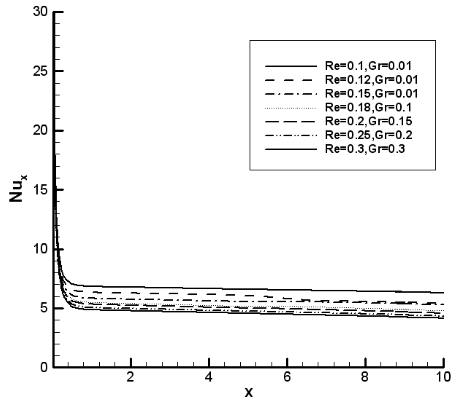

Fig. 15, Local Nusselt number through microchannl in case 3

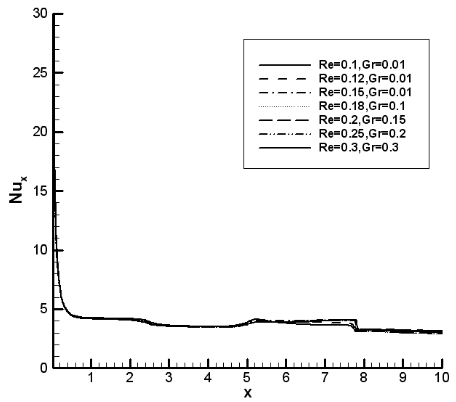

Fig. 16, Local Nusselt number through microchannel in case 4

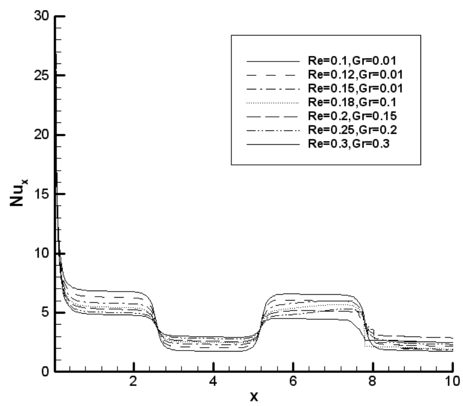

Fig. 17, Local Nusselt number through microchannel in case 5

As shown in previous figures by increasing the Reynolds number, the Nusselt number decreases rapidly, this decline is the straight result of decreasing momentum quality near the wall, where heat transfer occurs. It is observed that by increasing Grashof number from 0.01(the typical value in microchannels) up to 30 times, heat transfer only increases about 2%, that is in agreement with Avci and Aydin work, So the effect of buoyancy forces through vertical microchannels is negligible. The insignificant effect of buoyancy forces is

ISBN: 978-988-18210-7-2
ISSN: 2078-0958 (Print); ISSN: 2078-0966 (Online)

because of the very small length scale in microchannels (Grashof number is proportion to L^3).
In this part, pressure, stream function, vertical velocity, horizontal velocity contours, and velocity vectors are depicted for Re=0.1 and Gr=0.01 in first case study.

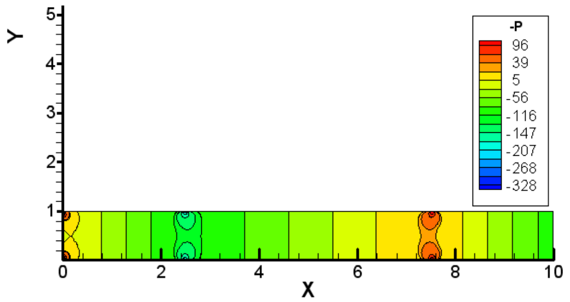

Fig. 18, Pressure contours through channel at Re=0.1, Gr=0.01

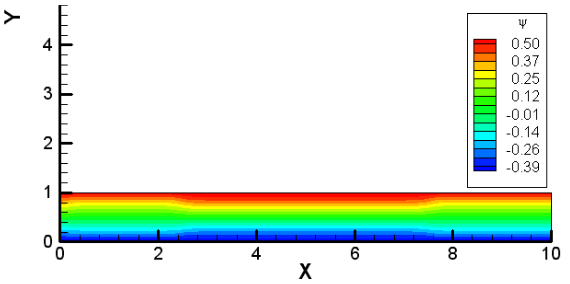

Fig. 19, Stream function contours through channel at Re=0.1, Gr=0.01

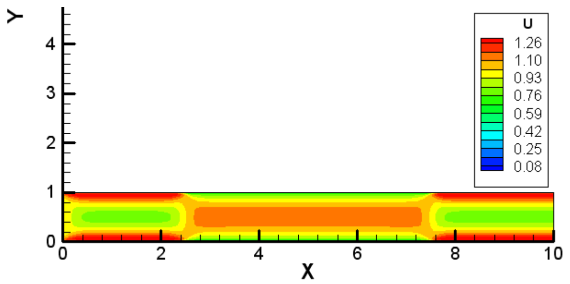

Fig. 20, Vertical velocity contours through channel at Re=0.1, Gr=0.01

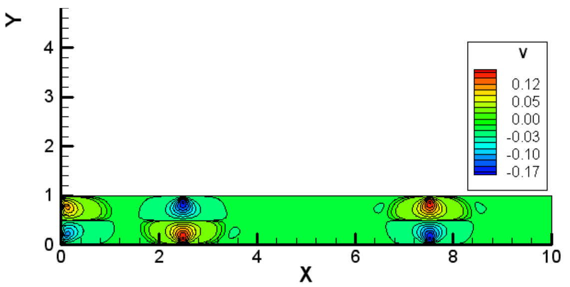

Fig. 21, Horizontal velocity contours through channel at Re=0.1, Gr=0.01

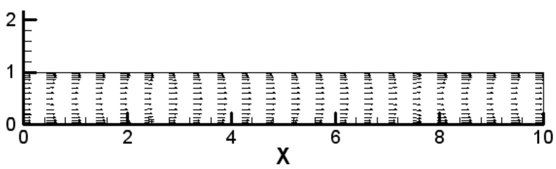

Fig. 22, Velocity vectors through microchannles at Re=0.1, Gr=0.01

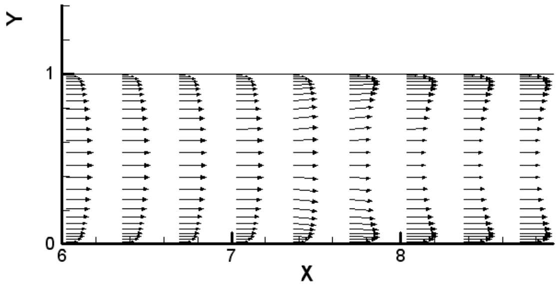

Fig. 23, Velocity vectors through microchannles at Re=0.1, Gr=0.01(nearview)

V. Conclusion

In this work, mixed convection through a vertical microchannels affected by EDL has been studied numerically. Generally EDL increases the momentum near the walls and makes high gradient velocity near walls. Increasing the momentum of fluid near the wall makes Nusselt number increases dominantly. Because of the vertical position of microchannels, the effect of buoyancy forces is considered using Boussinesq approximation. As shown, due to small length scale in microchannels contrary to macrochannels and consequently small Grashof number, buoyancy forces in real vertical microchannels is negligible. By increasing Reynolds number, fluid flow tends to take the parabolic shape (poiseuille flow) and the temperature gradient and accordingly the Nusselt number decrease. Because of high velocity gradient, viscous dissipation is important in microchannels. Viscous dissipation makes fluid warmer than usual and decreases the Nusselt number.

References

[1] George Karniadakis, Ali Beskok, Narayan Aluru, N., Micro flows and Nano flows: Fundamentals and Simulation, Springer-Verlag, New York, 2005.
[2] Y.H. Zhang, X.J. Gu, R.W. Barber, D.R. Emerson, An analysis of induced pressure fields in electroosmotic flows through microchannels, J. Colloid Interface Sci. 275 (2) (2004) 670–678.
[3] J.Y. Min, D. Kim, S.J. Kim, A novel approach to analysis of electroosmotic pumping through rectangular-shaped microchannels, Sens. Actuators B: Chem. 120 (1) (2006) 305–312.
[4] A.M. Afonso, M.A. Alves, F.T. Pinho, Analytical solution of mixed electro-osmotic/pressure driven flows of viscoelastic fluids in microchannels, J. Non-Newtonian Fluid Mech. 159 (2009) 50–63
[5] H. Bruus, Theoretical Microfluidics, Oxford Master Series in Condensed Matter Physics, Oxford University Press, Oxford, UK, 2008.
[6] F.F. Reuss, Sur un nouvel effet de l'électricité galvanique, Mémoires de la Societé Impériale des Naturalistes de Moscou 2 (1809) 327–337.
[7] H. Helmholtz, -ber den Einfluß der elektrischen Grenzschichten bei galvanischer Spannung und der durch Wasserstrmung erzeugten Potentialdifferenz, Ann. 7 (1879) 337.
[8] M. von Smoluchowski, Versuch einer mathematischen Theorie der Koagulationskinetic kolloid Lsungen, Z. Phys. Chem. 92 (1917) 129–135.
[9] G.M. Mala, Y. Chun, D.Q. Li, Electrical double layer potential distribution in a rectangular microchannel, Colloids Surf. A: Physicochem. Eng. Aspects 135 (1) (1998) 109–116.
[10] G.M. Mala, D.Q. Li, J.D. Dale, Heat transfer and fluid flow in microchannels, Int. J. Heat Mass Transfer 40 (13) (1997) 3079–3088.
[11] C. Yang, D.Q. Li, J.H. Masliyah, Modeling forced liquid convection in rectangular microchannels with electrokinetic effects, Int. J. Heat Mass Transfer 41 (24) (1998) 4229–4249.

ISBN: 978-988-18210-7-2
ISSN: 2078-0958 (Print); ISSN: 2078-0966 (Online)

[12] Hu, L., Harrison, J., and Masliyah, J. H., J. Colloid Interface Sci. 215, 300 (1999).
[13] Yang, C., and Li, D., J. Colloid Interface Sci. 194, 95 (1997).
[14] Yang, C., Li, D., and Masliyah, J. H., Int. J. of Heat Mass Transfer 41, 4229 (1998).
[15] Arulanandam, S., and Li, D., Colloids Surf. A 161, 89 (2000).
[16] R.-J. Yang,1 L.-M. Fu, and Y.-C. Lin, Electroosmotic Flow in Microchannels, Journal of Colloid and Interface Science 239, 98–105 (2001)
[17] Yih Nen Jeng, Jiann Lin Chen, On the Reynolds-Number independence of mixed convection in a vertical channel subjected to asymmetric wall temperatures with and without flow reversal, Int. J. Heat and Fluid Flow, Vol. 13, No. 4, December 1992.
[18] Aung, W. and Worku, G. 1986a. Developing flow and flow reversal in a vertical channel with asymmetric wall temperature. *ASME J. Heat Transfer,* 108, 299-304.
[19] Mete Avci, Orhan Aydin, Mixed Convection in a Vertical Parallel Plate Micro channel With Asymmetric Wall Heat Fluxes, ASME October 26, 2006.
[20] A. Barletta, M. Celli, Mixed convection MHD flow in a vertical channel: Effects of Joule heating and viscous dissipation, International Journal of Heat and Mass Transfer 51 (2008) 6110–6117.

ISBN: 978-988-18210-7-2
ISSN: 2078-0958 (Print); ISSN: 2078-0966 (Online)